Syngas Production in DRM by use Ni,Pd,Pt/CaO Catalyst with ZrO_2 as Promoter

Ali M. A. Al-Najar[1], Ali A. A. Al-Riyahee[1], Faris A. J. Al-Doghachi[1,*], Yun Hin Taufiq-Yap[2,3,*]

1. Department of Chemistry, Faculty of Science, University of Basrah, Basra, Iraq
2. Chancellery Office, University Malaysia Sabah, 88400, Kota Kinabalu, Sabah, Malaysia
3. Catalysis Science and Technology Research Centre, Faculty of Science, University Putra Malaysia, 43400, UPM, Serdang, Selangor, Malaysia

*Corresponding Authors: Faris A. J. Al-Doghachi, E-mail: farisj63@gmail.com, Yun Hin Taufiq-Yap, E-mail: taufiq@upm.edu.my

Doi 10.29072/basjs.20200106

Abstract

Through adopting the co-precipitation method using K_2CO_3Nickel, palladium and platinum catalysts (every 1 wt.%) On CaO and ZrO_2 to develop Pt,Pd and Ni /$Ca_{1-x}Zr_xO$ (where x = 0, 0.03, 0, 07 and 0.15) were manufactured. As a precipitate, X-ray diffraction (XRD), X-ray photoelectric spectroscopy (XPS), Brunauer-Emmett-Teller (BET), Transmission Electron Microscope (TEM), Programmed H_2 (H_2-TPR) and thermo-thermal analysis (TGA). Pt,Pd,Ni/$Ca_{0.85}Zr_{0.15}O$ reported best methane dry reform (DRM) activity at 98.02% and 85.94% for Carbon dioxide and methane conversions and 1.14 for H_2/CO- ratio at 900°C and 1:1 of CH_4:CO_2 ratio. Various effects were observed when ZrO_2 was used as a catalyst promoter. First, the cubic CaO stage has stabilized. Second, there was an increase thermal stability and basic support. In the end, carbon deposits and Ni^{2+}, Pd^{2+} and Pt^{2+} ions have shrunk.

Article inf.

Received: 13/4/2020

Accepted 20/4/2020

Published 30/4/2020

Keywords:

Biogas, Catalyst Deactivation, DRM, H2 Productio, Ni, Pd, Pt catalyst

1. Introduction

Because fossil fuel reserves run fast, so alternative energy resources are badly needed . Thus gases such as CH_4 and CO_2 are important alternative energy sources, as they are used as greenhouse gases . Methane is readily available. As the search for CH_4 ended with positive results, and it was found on larger reserves of crude oil reserves. The shale gas and fermenting waste can also be used to produce methane [1]. Methane is converted into syngas which is a mixture of H_2 and CO and through the use of steam, partial oxidation or CO_2 in DRM it can be produced. The process of converting methane and carbon dioxide to syngas takes place through dry reforming. These gases are very cheap and available, most of them contain carbon-containing materials such as methane, carbon dioxide and greenhouse gases. These materials have very important environmental effects in this reaction Eq.1, which can be converted into hydrogen as valuable product. Further, due to its large heat of reaction and reversibility, this process has potential thermo-chemical heat-pipe applications for the recovery, storage, and transmission of solar and other renewable energy sources.

$$CH_4 + CO_2 \longrightarrow 2CO + 2H_2 \quad \Delta H_{298}^{o} = 247.0 \text{ kJ/mol} \qquad (1)$$

Industrial gas is an important raw material for the production of chemicals used in industry or for the production of fuel. In fact, fossil fuels and biomass can become a synthetic gas. For use, for industrial application purposes of synthetic gas, with different molar ratios of H_2/Co. It was found that the ratio of H_2/CO equals 2 as an example for the formation of industrial gas from methanol [2] . When dimethyl ether dissociation in one step during the process of industrial gas formation, H_2/CO equals 1 [3,4]. The main controller in syngas production process is H_2/CO [5]. Noble elements such as Pt, Rh, and Ru are highly active when interacting with DRM [6]. In addition, it was found that these minerals are more effective in resistance compared to other transitional minerals to form carbon on the catalyst [7]. But nickel catalysts are more suitable with noble minerals such as Pd, Pt, Rh, Ru. It is more persistent in its reactions against coke precipitation and increases the reaction of catalysts compared to other inappropriate catalysts [8]. For example, it was found that the catalyst containing Ni, Pt supported by ZrO_2 is able to maintain a longer period of activity time compared to the Ni/ZrO_2 monometallic . Thus, the Ni, Pt catalyst has more potential for industrial application in a DRM reaction [9]. Besides, the three-metal catalysts Pt, Pd, and Ni are more active and stable than the mono-metal catalysts [10]. These results support

the idea that Pt-Pd can be used to prevent nickel oxidation . This reaction was caused by heterogeneity with CaO that caused an increase in the size of nickel particles [11]. The current paper describes the synthesis of catalysts Pt,Pd,Ni/$Mg_{1-x}La_xO$ (where x = 0, 0.03, 0.07, and 0.15), each of 1% of the Ni,Pd, and Pt included minerals, through common precipitation processes, evaluating their activity, stability selection, and ability to reduce carbon deposition in the DRM reaction on the catalyst. to gain insight into the effect of a factor on Pt,Pd,Ni-catalysts' using efficiency over a long time during a DRM reaction, XRD, XPS, BET, TEM, H2-TPR and TGA were used for both reduction and catalytic use. The catalyst used in comparison to previous work to strengthen the selectivity and stability [12].

2. Materials and Method

2.1 Materials

$ZrCl_4$ (aq) (99.0%), Ca $(NO_3)_2$.6 H_2O (99.0%) and K_2CO_3 (99.7%) were obtained from Merck Company. Pt $(C_5H_7O_2)_2.H_2O$ (99.0%) and Ni $(C_5H_7O_2)_2.H_2O$ (99.0%) were supplied by Acros chemicals Company. While Pd $(C_5H_7O_2)_2.H_2O$ (99.5%) was obtained from Aldrich company .

2.2. Preparation of catalysts

The Pt,Pd,Ni/CaO_{1-x} Zr_xO, (x =0.00, 0.03, 0.07, and 0.15).catalysts were prepared in the laboratory by Co- precipitation method. The support of CaO and promoter zirconia of ZrO_2 was prepared according to a literature method [12]. By using a0.1M $ZrCl_4$(aq) $Ca(NO_3)_2.6H_2O$ and 1.0 M K_2CO_3. After filtering the precipitate, the sample was washed with warm water, then dried at 120°C for 12 h. After that, a precipitate was calcined in the air at a temperature of 500 degrees to get rid of CO_2 gas for a period of 5 h. Then the sample was compressed with 600 kg/m^2 in tablet form. In order to demonstrate mechanical properties and ensure smooth interaction of CaO with ZrO_2, The material was calcinated for 20 h at 1150 °C. Steps were illustrated that included preparing the catalysts Ni, Pt, Pd $(acac)_2$ at a concentration of (1% for each Ni, Pd, Pt metal) where first 1% of Pt $(C_5H_7O_2)_2.H_2O$ was first used and dissolved in dichloromethane for 5 h. to produce Pt $(acac)_2/CaO_{1-x}$ Zr_xO . After that, the catalyst was impregnated with 1% Pd and Ni each. Pd $(C_5H_7O_2)_2$ and Ni $(C_5H_7O_2)_2.H_2O$ solutions were used in dichloromethane for 5 hours to

prepare the catalysts. The catalysts were dried at 120 °C for 12 h. after impregnation with air. Finally, catalysts are ground and screened in particles of 80-150 or 150-250 microns in diameter.

2.2. Characterization catalyst

Generally speaking, in this section, a light was shed on a diffractometer (Shimadzu model XRD6000), which was adopted in this study. The radiation process occurred in a 2.7 kW wide focus X-ray tube with Philips glass diffraction. The estimation of the crystal dimension is based on the relationship between Debye-Scherrer. [13]. A monochrome Al Kα (1486.6 eV), and two X-ray sources (Al&Mg) were connected to the Kratos Axis Ultra DLD system. An emission current of 20 mA combined with 15 kV tension is used to operate the X-ray gun that is the source of excitement. The mode is based on a fixed analyzer transmission (FAT) for large and small scanning for this hemispheric analyzer. At 100 eV and 40 eV the power was set. Interesting region of the Mg2p, La3d, Pd3d, Ni2d, Pt4f and O1 scanning and photoelectron signals are mutually compatible. Carbon recharge refers to 285 eV binding capacity for adventitious carbon. The measurement of the active site of the catalyst was performed using the H2-TPR method of temperature declination involving hydrogen.

The Thermo Finnegan TPDRO 1100, along with a thermal-conductivity detector, was used as an apparatus to test. In Brunauer-Emmett-Teller (BET), the catalyst 's total area was measured using a nitrogen adsorption at -196°C. In the meantime, the nitrogen adsorption-desorption analyzer Thermo Fisher Science S.P.A has been adopted for research Model: Surfer Analyzer. Diagnosing the crystal-system and the catalyst's homogeneity by the unit, transmitting electron micro (TEM) (Hitachi H7100, TEM with an. voltage of 10 MV).

In general, Mettler Toledo TGDTA (Pt cruples, Pt / Pt-Rh thermocouple) and a heating range of 50-1000 degrees Celsius were used to conduct thermosgravimetric analysis (TGA).

3. Results and Discussion

3.1 Characterization of the catalysts

3.1.1 XRD patterns

Catalysts contain CaO and ZrO_2 are shown in Fig.1 (a-d) XRD patterns. Diffraction values have been observed at 2θ = 23.2°, 29.5°, 35.9°, 39.5°,43.2°, 47.2°, 48.5°, 64.7°, and 65.6°. These values are attributed to the cubic shaped calcium oxide (JCPDS file no.: 00-002-0629).

Meanwhile, the peaks recorded at 2θ =22.19°, 31.1°, 31.5°, 33.9°, 50.8°, 55.5°, 56.7°, 65.8°, and 74.75°. Were due to the cubic form of ZrO_2 (JCPDS file no.: 00-003-0719). Due to the cubic (Ca-zr-O) catalysts the peaks recorded at 2θ = 11.6 °, 11.7 °, 17.8 °, 28.6 °, 45.1 ° and 62.3 ° were most common . As for catalysts containing 1% of Pt, Pd, Ni, there were no diffraction values in all patterns. The absence of diffraction peaks is due to the use of a very small amount of metal in the catalyst, where the percentage used for the metal is 1%. This comment was close to Grange 's conclusions [14]. Using the Debye-Scherrer equation, maximum diffraction of XRD patterns was determined. Whereas the diffraction values obtained from the equation were used to determine the average size of the crystalline. We observe an inverse proportion between the crystal size and the increasing amount of ZrO_2 in the catalysts through the results calculated in the Debye-scherrer equation. This is happened by reducing Pt, Pd, Ni on a surface of a sample that leads to the growth of calcium oxide crystals. The crystal size for the following catalysts was 41.0, 43.2, 39.2 and 37.2 nm,

(a) Pt,Pd,Ni/CaO, (b) **Pt,Pd,Ni/$Ca_{0.97}Zr^{4+}_{0.03}O$,** (c) **Pt,Pd,Ni/$Ca_{0.93}$ $Zr^{4+}_{0.07}O$**, and (d) **Pt,Pd,Ni/ $Ca_{0.85}$ $Zr^{4+}_{0.15}O$** , respectively:

On that account, the cubic crystal system is the most prevalent of all the samples. This outcome is confirmed by cubic particles observed by TEM.

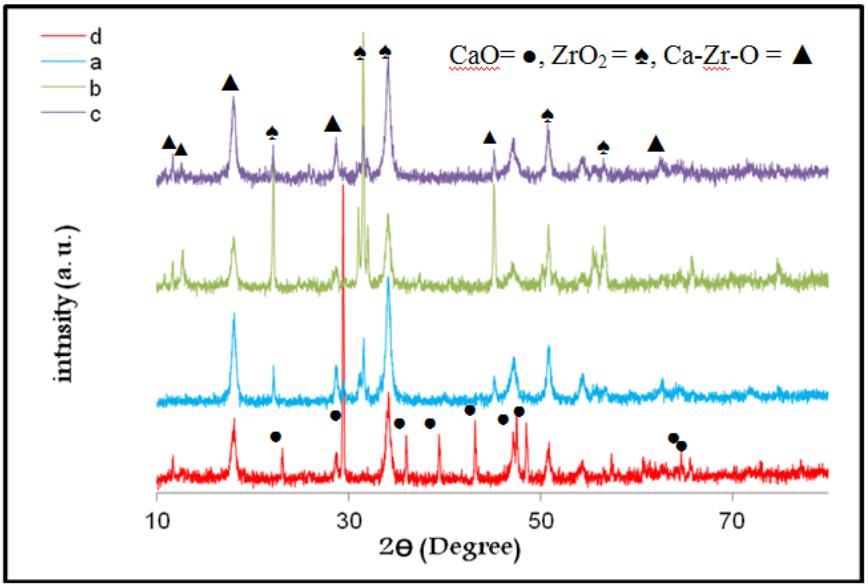

Fig. 1: XRD patterns of the catalysts : **(a)** Pt,Pd,Ni/CaO**, (b)** Pd,Pd,Ni/ $Ca_{0.97}Zr^{4+}_{0.03}O$ **, (c)** Pd,Pd,Ni/ $Ca_{0.93}Zr^{4+}_{0.07}O$**, (d)** Pd,Pd,Ni/ $Ca_{0.85}Zr^{4+}_{0.15}O$

3.1.2 H_2-TPR

The following catalysts were examined for their reductive behaviour by TPR Pt,Pd,Ni/CaO (a) Pt,Pd,Ni/$Ca_{0.97}$ $Zr^{4+}{}_{0.03}O$ (b) Pt,Pd,Ni/ $Ca_{0.93}$ $Zr^{4+}{}_{0.07}O$ (c) Pt,Pd,Ni/$Ca_{0.85}$ $Zr^{4+}{}_{0.15}O$ (d) Fig. 2 a-d and Table 1 showing the features of TPR for these catalysts. fig. (2a) The TPR profile of Pt,Pd,Ni/CaO showed three well defined reduction peaks. At 126 °C was the first reduction peak. This result describes the PtO reduction in the production of Pt°, compared to Mahoney et al. [15] that identifies PtO species reduction at 114 °C. For the second peak at 145 °C, PdO will be reducing back to Pd°. As for the final peak, the strong overlap of materials supporting production of Ni was recorded in the temperature range of 557 ° C. This can occur in few types of nickel oxide. In a study conducted by Bao *et al*. [16], The NiO for the Ni/ZrMgAl catalyst is observed to be reduced at 516 °C. Fig. 2 b-d and Table 1 extend the ZrO_2 promoter TPR catalyst profile. The catalyst TPR file (fig. b, c, and d) are not same to that of the catalyst of Pt,Pd,Ni/MgO. One of the divergences rests on the number of peaks. Five peaks revealed results. The first three peaks of the Pt,Pd,Ni/ $Mg_{0.97}La_2{}^{3+}{}_{0.03}O_3$ catalyst were recorded at 117, 157, and 413 °C. The catalyst of the Pt,Pd,Ni/$Mg_{0.93}La^{3+}{}_{0.07}O_3$ demonstrated peaks at 121, 159, and 435 °C, while peaks of the Pt,Pd,Ni/ $Mg_{0.85}La^{3+}{}_{0.15}O_3$ catalyst was discovered at 108, 162 and 405°C. This is due to the reducing in PtO, PdO, and NiO through the surface layer of the catalyst to gain the Pt°, Pd°, and Ni° elements, respectively. As far as the fourth peak of the catalyst (fig. b, c, and d) is concerned, it was recorded at a temperature were 541, 570 and 573°C, respectively. The returns concur with the shortened amount of ZrO_2 on the surface. There are some basics that explain this event. Through MgO integration and the lateness of sintering process the first basic could be connected to the well-distributed ZrO_2 particles [17]. The other basic may describe the interference among ZrO_2 , Pt, Pd and Ni metals behave vigorously during the overlapping of PtO, PdO, NiO, and ZrO_2 when they share the peaks. At 606, 621 and 622°C respectively, the fifth peak was composed. There are strong interactions between ZrO_2 species and CaO help with reduced ZrO_2 size. When the promoter load increased, the catalysts show a high degree of reduction ability. This was similar to the results of previous studies. Roberto, *et al.* [17]. Lanthanum was reduction at 490 and 790 °C It was reported. The returns of the promoters also revealed that the supporting and the interaction between the support for Pt , Pd and Ni loaded species was strong. Another result reported in the TPR file was that it had a large peak that appeared at a temperature ranging from 684 to 737°C. Therefore, ZrO_2 alone was able to reduce the temperature [18]. The addition of

ZrO_2 promoter was also found to increase the reducibility of MgO-supported catalysts. A more contact with the ZrO_2 promoter is evident from Ca1-x Zr^{4+}xO, which has more simple than CaO. As a consequence, the redox property of Ca1-x Zr^{4+}xO has reduced PtO, PdO, and NiO significantly [19]. In the process of reducing the catalysts (fig. a, b, c, and d) the total amount of H_2 absorbed was determined by the total peak area. For the catalysts 511.3, 763.1, 862.6 and 993.3 µmol / g respectively, the measurement was reported. The most active catalyser according to H_2-TPR results was PT,Pd,Ni/$Ca_{0.85}Zr^{4+}{}_{0.15}O$, suggesting the most appropriate DRM reaction catalyst.

Table 1: H_2-TPR values of the different catalysts

Catalysts	Temp. °C	Temp. °C	Temp. °C	Temp. °C	Temp. °C	Amount of Adsorbed H_2 gas (µmol/g)
Pt,Pd,Ni/CaO	126	145	557	-	-	511.3
Pt,Pd,Ni/$Ca_{0.97}$ $Zr^{4+}{}_{0.03}O$	117	157	413	541	606	763.1
Pt,Pd,Ni/ $Ca_{0.93}$ $Zr^{4+}{}_{0.07}O$	121	159	435	570	621	862.6
Pt,Pd,Ni/ $Ca_{0.85}$ $Zr^{4+}{}_{0.15}O$	108	162	405	573	`622	993.3

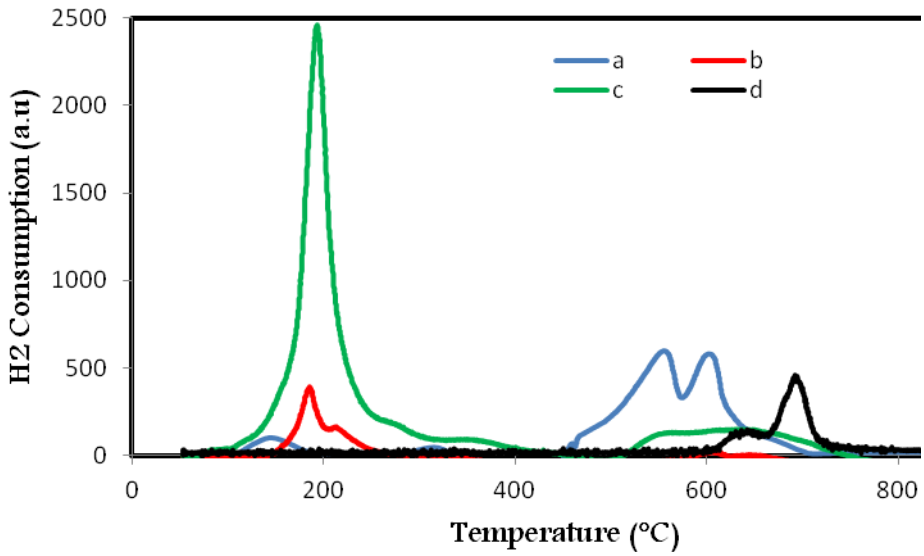

Fig. 2:H_2-TPR profiles of catalysts reduced in a (5 % H_2/Ar) stream at a temperature ramp of 10 °C/min

3.1.3 BET surface area

Table 2 shows the pore radius, pore-volume, and surface area of the support CaO and for the Pt,Pd,Ni/$Ca_{1-x}Zr_xO$ catalysts (where x =0.00, 0.03, 0.07, and 0.15). The Pt,Pd,Ni/CaO catalyst with a TEM-supported cubic construction recorded a surface area at 14.06 m^2/g. As for the CaO-supported surface area was 12.1 m^2/g recorded. The former recorded the effect of Pt , Pd, and Ni loads on the fixed surface of the CaO support with a higher value . At that state, the Pt, Pd, Ni /CaO surface areas, at 15.04, 16.55 and 19.35 m^2/g respectively, were substantial lower than the classic catalyst (b, c and d). The main motive of this condition is the presence of layers of Pt, Pd, Ni particles that moderately contain the pores of magnesia.. The BET surface of CaO stimulated by ZrO_2 was almost identical to a common binary supporting Pt, Pd and Ni catalyst [20]. Meanwhile, very low metal distribution and small areas of Pt and Pd with small Ni particles were formed by the lineaments of the supported Pt , Pd and Ni catalysts of a cubic structure. The result is that the CaO supports ZrO_2 promoters with remarkably reactivity between the Pt,Pd, and Ni layers. The pore volume was 0.037 and 0.052 cm^3/g , respectively, of the catalysts Pt, Pd,Ni/$Ca_{0.93}Zr^{4+}_{0.07}O$, partially less than the pore volume Pt, Pd ,Ni was 0.066 cm^3/g Pt,Pd,Ni/$Ca_{0.85}Zr^{4+}_{0.15}O$ was the catalyst of the catalyst pore. Such findings varied from Faris et al 's analysis [21], Where $Zr_{1-x}Ca_xNiO_3$ catalyst pore volume amounted to 0.51 cm^3/g. Table 2 showed the pores of different catalysts. The CaO support pore radius was 9.9, Å while the Pt, Pd, Ni / CaO

catalyst pore radius was 28.48 Å . The radius of the other catalysts is mutually proportional and that of the promoter ZrO_2 is growth. The pore radius of the catalysts (b, c, and d) were 39.40 Å, 33.15 Å, and 21.30 Å, respectively [22]. Those data tend to be the strongest operation in DRM reaction in contrast to other catalysts for Pt,Pd,Ni/$Ca_{0.85}Zr^{4+}_{0.15}O$ catalyst with a high surface area.

Table 2: The main textural properties of fresh catalysts

Sample name	Specific surface area (m^2/g)	Pore volume (cm^3/g)	Pore radius (Å)
CaO	12.1	0.22	9.9
Pt,Pd,Ni/CaO	14.06	0.13	28.48
Pt,Pd,Ni/$Ca_{0.97}Zr^{4+}_{0.03}O$	15.04	0.037	39.40
Pt,Pd,Ni/$Ca_{0.93}Zr^{4+}_{0.07}O$	16.55	0.052	33.15
Pt,Pd,Ni/$Ca_{0.85}Zr^{4+}_{0.15}O$	19.35	0.0.66	21.30

3.1.4 TEM characterization

Figure 3.a-d illustrate TEM photo of Pt,Pd,Ni/CaO (a), Pt,Pd,Ni/$Ca_{0.97}Zr^{4+}_{0.03}O$ (b), Pt,Pd,Ni/ $Ca_{0.93}Zr^{4+}_{0.07}O$ (c), and Pt,Pd,Ni/$Ca_{0.85}Zr^{4+}_{0.15}O$ (d) Cubic form catalysts. At 1150 °C the catalysts underwent a calcination process without the use of free ZrO2 with uniform particle distribution .The formation of solid solutions [23], CaO-ZrO_2 is seen on the Pt , Pd and Ni layers of the sponsored metal by figures from a-d with cubic form oxide molecules. Catalyst Pt, Pd, Ni/ $Ca_{0.85}Zr^{4+}_{0.15}O$ Fig.3d. 1% dispersion of Pt, Pd and Ni metal particles for each carrier of CaO-ZrO_2 in sizes in the range from 45 to 85 nm . As well, TEM analysis showed induced growth with nanoparticle agglomeration on a specific area between the mineral crystals in the catalyst Pt,Pd,Ni/$Ca_{0.85}Zr^{4+}_{0.15}O$ The distribution of image sizes in TEM demonstrated more specificity and precision, as the metallic Pt, Ni and Pd stimulates this form of development [24]. Fig.3 a-d

exhibits the TEM results that match the XRD data. These results demonstrated that not only was Ca–Zr –O complex, but also cubic, similar to CaO and ZrO.

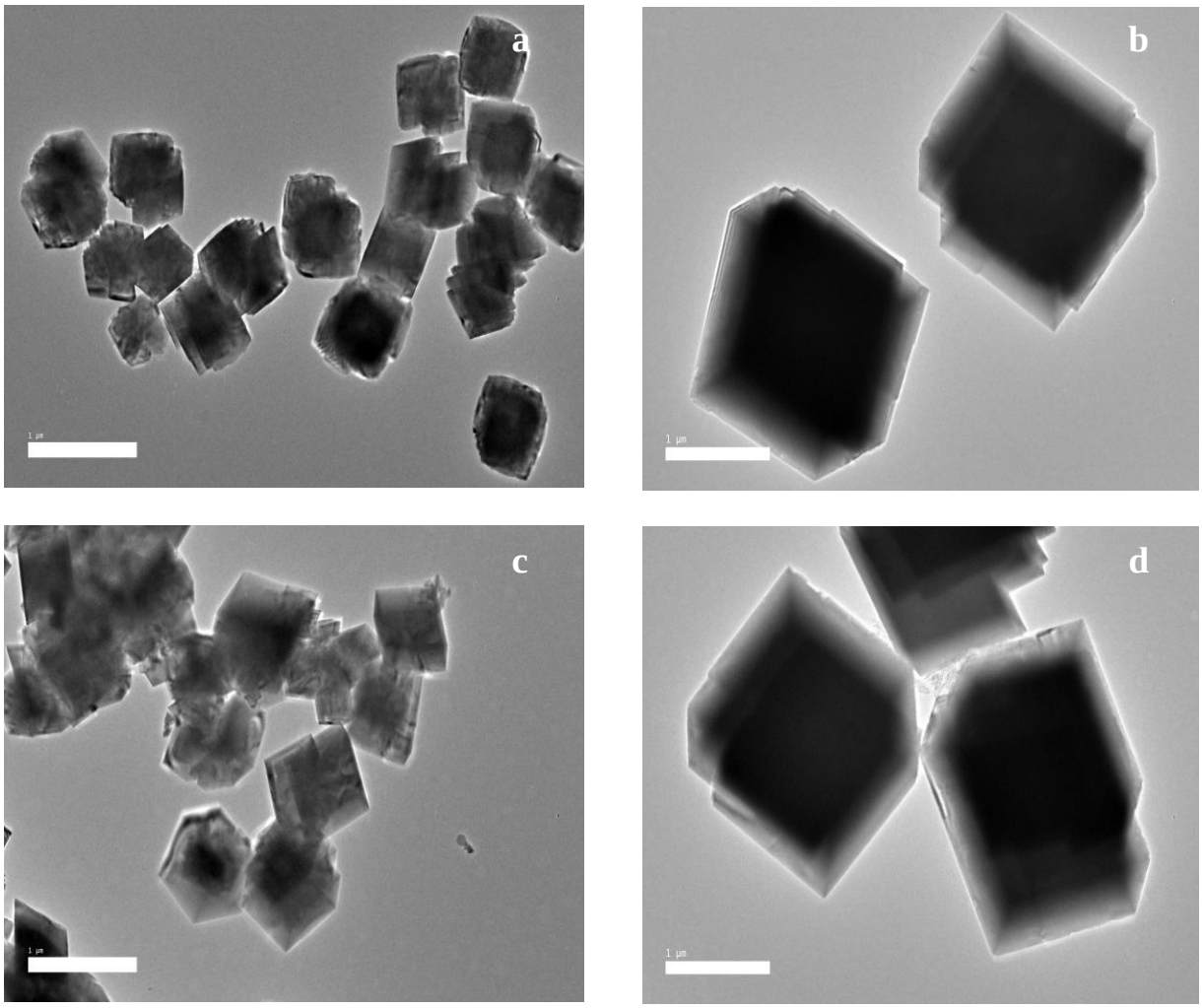

Fig.3: TEM image of catalysts, **(a)** Pt,Pd,Ni/CaO, **(b)** Pt,Pd,Ni/$Ca_{0.97}Zr^{4+}_{0.03}O$, **(c)** Pt,Pd,Ni/$Ca_{0.93}Zr^{4+}_{0.07}O$, **(d)** Pt,Pd,Ni/ $Ca_{0.85}Zr^{4+}_{0.15}O$,

3.1.5 Thermal analysis

Figure 4. a-d explain TGA for the Pt,Pd,Ni/CaO (a), Pt,Pd,Ni/$Ca_{0.97}Zr^{4+}_{0.03}O$ (b), Pt,Pd,Ni/ $Ca_{0.93}Zr^{4+}_{0.07}O$ (c), and Pt,Pd,Ni/ $Ca_{0.85}Zr^{4+}_{0.15}O$ (d) catalysts. Results obtained in thermal processes indicated weight loss, and that occurred in only one stage . 30% the amount of weight loss in relation to catalysts a, b, c and d at temperatures from 423 to 433°C . The result was due to the elimination of the Pt,Pd,Ni/$Ca_{1-x}Zr_xO$ catalyst from the calcium hydroxide. Involve weight loss at 18.9, 17.6, 7.2, and 15.9%, respectively. On the other hand, Pt,Pd,Ni/CaO (a), Pt,Pd,Ni/

$Ca_{0.93}Zr^{4+}_{0.07}O$ (b) catalysts see Fig. 4 c, d with more weight loss at 18.9 and 17.6%, respectively. This effect is due to the removal of O_2 atoms from the catalyst . Preliminary results revealed through the graph that the full of compound weight shows a small increase, owing to the nitrogen gas that is found in the engine adsorbed . At 600°C all the samples stay stable. This result was due to the more melting point of calcium oxide and ZrO_2 at 2572 and 2177 °C, respectively. From Figure 4.a-d, the catalyst components interacted well with each other. These results are similar to those of Komarala et al.[25].

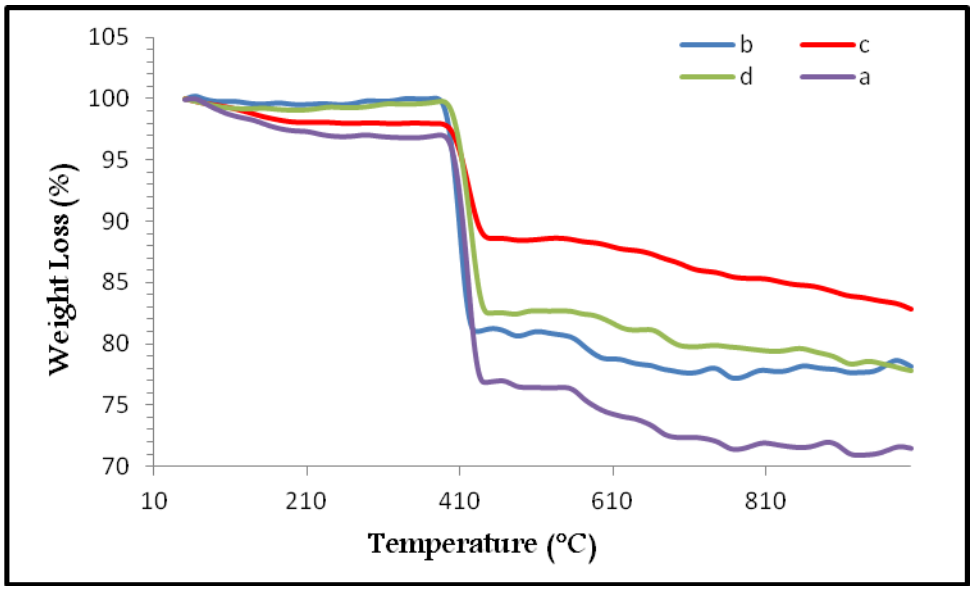

Fig. 4: TG of the catalysts: **(a)** Pt,Pd,Ni/CaO , **(b)** Pt,Pd,Ni/$Ca_{0.97}Zr^{4+}_{0.03}O$, **(c)** Pt,Pd,Ni/$Ca_{0.93}Zr^{4+}_{0.07}O$, **(d)** Pt,Pd,Ni/$Ca_{0.85}Zr^{4+}_{0.15}O$

3.2 Catalytic performance in biogas reforming

3.2.1 Effects of concentration of catalyst on conversion

The effect of changing catalyst concentration levels can be illustrated by fig. 5 and table 3 during the conversion process . The catalysts are arranged according to their conversion ability methane, carbon dioxide and H_2/CO ratio as follows , Pt,Pd,Ni/CaO < Pt,Pd,Ni/$Ca_{0.97}Zr^{4+}_{0.03}O$ < Pt,Pd,Ni/$Ca_{0.93}Zr^{4+}_{0.07}O$ < Pt,Pd,Ni/ $Ca_{0.85}Zr^{4+}_{0.15}O$. The key catalysts, namely, Pt and Pd with Ni and the support, CaO- $Zr^{4+}O_2$ were combined together. At a pressure of 1 atm and temperature 900°C with a reaction ratio (1:1) experiments were performed to convert (CH_4:CO_2) as in fig. 5 and table 3. The highest reading of 85.94% was recorded for the catalyst Pt,Pd,Ni/$Ca_{0.85}Zr^{4+}_{0.15}O$ in methane conversion, whereas the lowest reading was 83.28% for the catalyst Pt,Pd,Ni/CaO .

Results after 200 hours revealed that many of the promoted catalysts showed slight deactivation . In general, the process of converting carbon dioxide is more stable than converting methane. The highest rate of CO_2 conversion ratio was recorded by the catalyst Pt,Pd,Ni/$Ca_{0.85}Zr^{4+}_{0.15}O$ where it was 98.02% while the catalyst Pt, Pd,Ni/CaO showed the lowest conversion rate where the ratio was 96.16% . It was found that the more effective catalyst in the conversion operations is Pt,Pd,Ni/ $Ca_{0.85}Zr^{4+}_{0.15}O$ through the results obtained. Fig. 5 and table 3 show the H_2/CO ratio value which was more than (1). The process of converting carbon dioxide using Ni metal only was less positive compared to those three-metal catalysts, and this is what the results indicated in previous studies.[15] However, evidence of change in side reactions suggested by discrepancies between conversions and product performance was observed. When the increase in the level of the concentration of zirconium oxide as shown in table 3 ,the conversion its increase in rate of CH_4 and CO_2 as well as the H_2/CO ratio is followed. The Pt, Pd and Ni/$Ca_{0.85}Zr^{4+}_{0.15}O$ catalytic converter delivers excellent on-site results with the majority of H_2-TPR activities and excellent BET results on a large surface area. This event shows that adding ZrO_2 to CaO catalysts can significantly reduce the reverse water gas reaction (RWGS) to EQ.8.

$$CO_2 + H_2 \longrightarrow CO + H_2O \qquad \Delta H^o_{298} = 41.0 \text{ kJ/mol} \qquad (8)$$

The results showed that the heavy interference between the ZrO_2 promoter and the CaO support in the solid solution affects the rate of CO_2 formation in the DRM reaction. The findings are as follows: the molar ratio in the catalyst is 0.15:0.85, the maximum surface area is (19.35) m2 / g and the location with the highest operation is (993.3) µmol / g of the total quantity of H_2-Evidence of consumption for the H_2-TPR test is given. Table 1 . The process of building a solid solution was therefore critical for the development of active CO_2-reforming methane centers. The presence of the full promoter ZrO_2 as a solid solution stabilized the two oxides. When hydrogen was reduced at 700 °C, the CaO-ZrO_2 catalyst only shrank the surface layer of the solid ZrO_2 solution . Moreover, An obstacle to Zr sintering occurs because Zr locations remain close to the solid solution [26]. In addition, locations that impaired the catalytic process were located in Pt, Pd and Ni particles, which induced extensive contact between the molecules Pt , Pd, Ni and CaO-ZrO_2. When the concentrations of Pt, Pd and Ni in the carrier increased, the conversion and selectivity of CH_4 and CO_2 showed no significant change. This can be due to the development of nanoparticles, which is the product of XRD (the equation of Debye-Sherrer) and TEM Table 2 tests. Although X-ray diffraction has been used for a simplified and possible estimate of the crystal size from the expansion of X-ray diffraction reflections using the Scherrer equation,

nanoparticles have been preferred for particles . Increasing the surface area and securing more reactions was done by selecting nanoparticles as catalysts in this study . In addition, these catalysts have the ability to effectively disperse Pt, Pd and Ni metals on the catalysts surface . These catalysts also form Lewis bases with the support metal oxide . In addition, increased support for the Lewis bases improved the catalyst's ability to absorb CO_2 in the DRM reaction. Afterwards, carbon dioxide production resulted as the adsorbed CO_2 interacted with dissolved carbon eq. 9 Or less than a coke.

$$CO_2 + C \longrightarrow 2CO \qquad \Delta H^o_{298} = {}^{+}172 \text{ kJ/mol} \qquad (9)$$

Carbon precipitation is prevented or reduced using CaO which is a strong base and has high absorption of carbon dioxide . In addition, lesser zirconium particulates are often formed in the upper layer compared to the non-adulterated ZrO_2 particles, due to the difficulty of reducing the solid ZrO_2- CaO solution [27,28]. When the foundations of the surface combine with small metal particles, the CaO-based solid catalyst can more effectively prevent carbon deposition . There are many obstacles in TEM images, despite the most realistic and accurate distribution . Since particle size is involved in the reactive behavior, the best readings were obtained for CH_4 and CO_2 conversion . In addition, steroid minerals Pt, Pd and Ni were produced on the basis of the Debye-Sherrer equation and the support of TEM analysis. The metal was as large as nanoparticles. The particle size therefore is important for reaction activity. Other results showed that when the particle size was reduced to a nanoscale, an increase in the conversion of the reactive and selective substances was observed. The results of other activities recorded at 993.3 μmol/g in the active sites and 19.35 m^2/g in surface tables 1 and 2 supported this result.

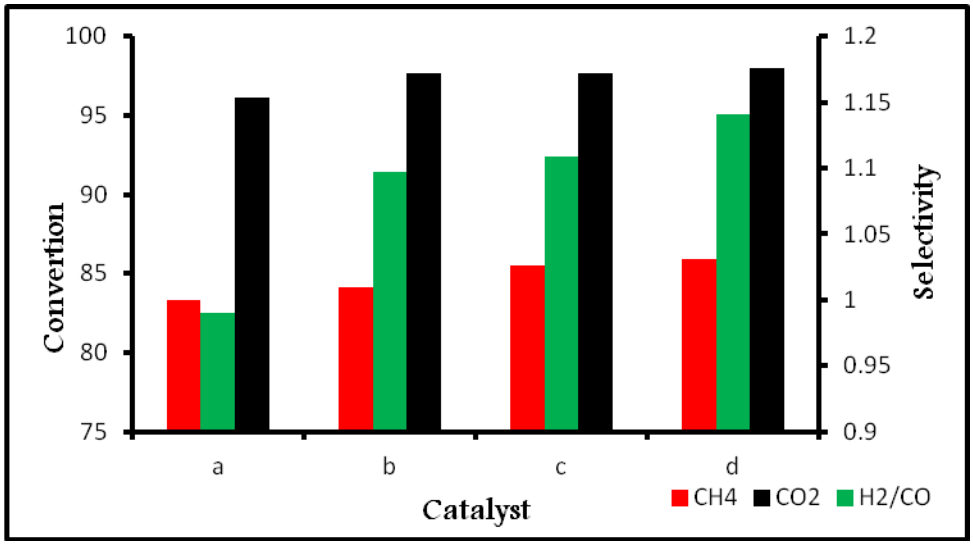

Fig.5. The effect of using different catalysts **(a)** Pt,Pd,Ni/CaO, **(b)** Pt,Pd,Ni/ $Ca_{0.97}Zr^{4+}_{0.03}O$, **(c)** Pt,Pd,Ni/$Ca_{0.97}$ $Zr^{4+}_{0.07}O_3$**,** and **(d)** Pt,Pd,Ni/$Ca_{0.85}$ $Zr^{4+}_{0.15}O$, on CH_4, CO_2 conversion and H_2/CO ratio at 900 ^oC for the 1:1 ratio of CH_4:CO_2

Table 3: The catalytic results of DRM reaction for the catalysts at 900 ^oC for the (1:1) ratio of CH_4: CO_2

Catalyst	CH_4 Conversion %	CO_2 Conversion %	H_2 / CO Conversion %
Pt,Pd,Ni/CaO	83.28	96.16	0.99
Pt,Pd,Ni/$Ca_{0.97}Zr^{4+}_{0.03}O$	84.12	97.64	1.09
Pt,Pd,Ni/$Ca_{0.93}$ $Zr^{4+}_{0.07}O$	85.52	97.65	1.10
Pt,Pd,Ni/$Ca_{0.85}$ $Zr^{4+}_{0.15}O$	85.94	98.02	1.14

3.2.2 Effects of temperature on conversion

At a temperature of 700-900°C, selective results and catalyst activity Pt, Pd, Ni/$Ca_{0.85}Zr^{4+}_{0.15}O$ are shown as in fig. 6. When the temperature increases from 700-900 °C, the conversion ratio (1:1) CO_2: CH_4 increases . The strong endothermic reaction like eq.1 and a greater temperature increase during DRM led to an increase in the conversion ratio CH_4:CO_2. In earlier work this phenomenon was recorded [29]. If a temperature of 700-900 °C was reached, the methane conversion rate increased from 51.75-85.94% for the catalyst Pt,Pd,Ni/$Ca_{0.85}Zr^{4+}{}_{0.15}O$. The same applies to the conversion of carbon dioxide, which increased from 73.53-98.02%. While there was no significant increase in methane and carbon dioxide conversions for temperatures in excess of 900°C . Fig.8 displays the catalyst H_2/CO ratio at different temperatures. The H_2/CO ratio of the samples was less than 1 when the temperatures were below 900°C . The result was eq.8 (RWGS). More H2 was used when CO was manufactured and the H_2/CO ratio was decreased. The H_2/CO ration for Catalyst Pt ,Pd,Ni/ $Ca_{0.85}Zr^{4+}{}_{0.15}O$ was 1,14 when the temperature was 900 °C, and this result shows that the response was eq. 8 (RWGS) has a minor effect [30]. Because the CO concentration will remain low while the hydrogen concentration will rise, then the H_2/CO ratio will be high.

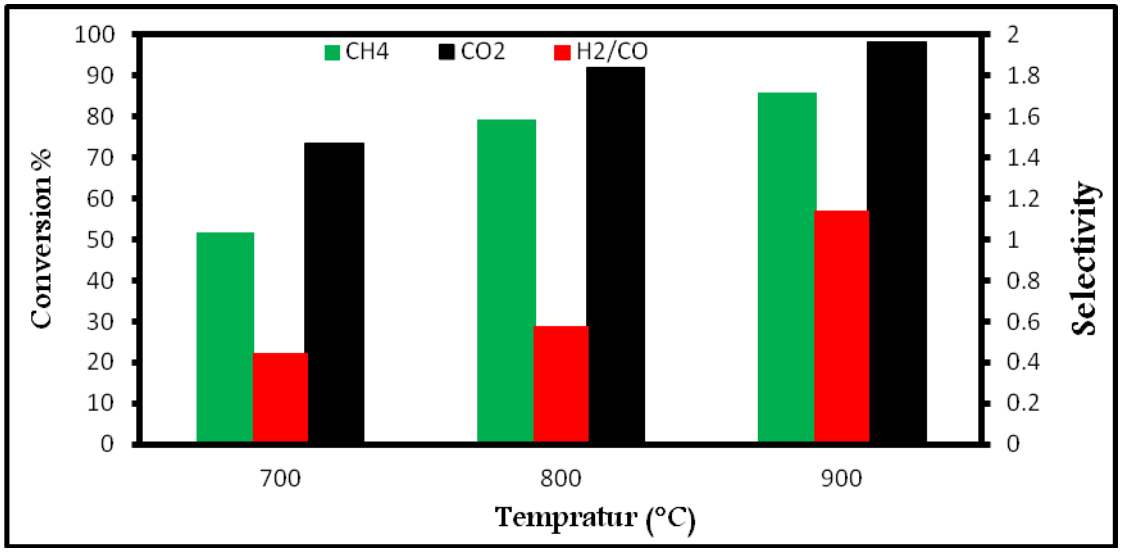

Fig. 6: The influence of temperature on the catalytic activity of the Pd,Pd,Ni/$Ca_{0.85}Zr^{4+}{}_{0.15}O$ catalyst, (1) **700 ºC**, (2) **800 ºC**, (3) **900 ºC** for the 1:1 ratio of CH_4:CO_2

3.2.3 Stability tests

The result getting from the test which includes temperatures is shown in fig. 7. At a temperature of 900°C, the results showed that the conversion rate of CH_4 and CO_2 was high because nickel has the best conversion compared to other minerals due to its size and high density of positive charge, so the mechanism is the interaction between the methane molecule and the nickel surface [31]. Desorbed species of hydrogen and CH_x (x=0 -4) produced; carbon deposits on the Ni-metal surface, if x=0, CH_x produced [32]. Eq. 10-14. are shown below:

$$CH_4 + 2Ni_{(as)} \longrightarrow CH_3Ni_{(as)} + HNi_{(as)} \quad (10)$$

$$CH_3Ni_{(as)} + Ni_{(as)} \longrightarrow CH_2Ni_{(as)} + HNi_{(as)} \quad (11)$$

$$CH_2Ni_{(as)} + Ni_{(as)} \longrightarrow CHNi_{(as)} + HNi_{(as)} \quad (12)$$

$$CHNi_{(as)} + Ni_{(as)} \longrightarrow CNi_{(as)} + HNi_{(as)} \quad (13)$$

$$2HNi_{(as)} \longrightarrow H_2 + 2Ni_{(as)} \quad (14)$$

as = (active side)

Metal active site Nakamura et al.[33] Identified the effects of a promoter on the catalyst during DRM by increased Pt , Pd and Ni dispersion. Activation of CO_2 on a support-promoter mixed with mineral particles to form carbonate types is one of the indicated effects. Subsequently, to form carbon monoxide the CHx species reduced the carbonate substrate eq. 15-19.

$$CO_{2\,(g)} \longrightarrow CO_{2(support)} \quad (15)$$

$$CO_{2(g)\,(support)} + O^{-2}_{(support)} \longrightarrow CO_3^{-2}{}_{(support)} \quad (16)$$

$$2H_{(metal)} \longrightarrow 2H_{(support)} \quad (17)$$

$$CO_3^{-2}{}_{(support)} + 2H_{(support)} \longrightarrow HCO_2^{-1}{}_{(support)} + OH^{-1}{}_{(support)} \quad (18)$$

$$CO_{(support)} \longrightarrow CO_{(g)} \quad (19)$$

It is recognized that the catalyst decreases its stability when depositing carbon on the metal surface, but the catalyst is activated with the presence of ZrO_2 that removes the deposited carbon . When carbon dioxide and methane as well as the H_2/CO ratio are converted for 200 hours or more, we will have coke, so to resist the formation of coke and provide a very stable platform, a ZrO_2 promoter should be present mainly in the catalyst. During the DRM reaction the carbon formed on the catalyst was removed by ZrO_2. Furthermore, in the presence of ZrO2, improved CO2 adsorption could increase the basis. The development of carbonate material, in particular ZrO_2, was accompanied by this process and could break down CO_2 to CO and O. The atom O is eventually moved to the promoter Zr. The precipitate is deposited on the metal catalyst CO in the

final stage resulting from the O atom with the precipitated [34]. Based on the results, the catalyst has demonstrated a significant decline in carbon deposition

eq. 20-21.

$$CO_{2(g)} \longrightarrow CO_{(support)} + O_{(promoter)} \quad (20)$$

$$C_{(metal)} + O_{(promoter)} \longrightarrow CO_{2(g)} \quad (21)$$

The conversion rate of both CH_4 and CO_2 decreases in the case of a high concentration of ZrO_2, but in the case of a decrease in the concentration of zirconium oxide, it indicates a conversion of CO_2 in active formation of strong ionic oxides like $ZrO.CO_3$, attracting CO_2 to the top catalyst layer, and increasing the conversion rate CH_4 thereafter . The high electronic density Pt, Pd, Ni can cause a decrease in ZrO_2 concentration [35]. The decomposition of $ZrO.CO_3$ species in DRM led to the production of carbon dioxide and the types of oxygen that interact with Pt, Pd and Ni-$ZrO.CO_3$ carbon deposits, reliving Pt, Pd and Ni sites of activity. Adsorbed carbon dioxide was also facilitated by the ZrO_2 supported catalysts. The separation of lanthanum adsorption improves the dispersion stability of small mineral particles, in addition to its promotional effect on CO_2. Zirconium is essentially an oxide that has been shown to react strongly during the supporting process of minerals, and significant surface properties changes have occurred, in both oxides and minerals [36]. It was found that mono-metallic catalysts such as Ni or Ni-Pd as well as with bimetallic catalysts such as Ni-Pt were less active and stable compared to three-metal catalysts Ni, Pd, Pt with high results as in table 2 and fig. 6. This can be attributed to the fact that Pt and Pd are working to transfer the electronic density to the metal Ni, which is the main catalyst in the triple catalyst, as explained in the previous work. This result is compatible with the theory of nickel oxidation by Pt and Pd thus increasing the electron density. [37,38]. The reducibility of Ni increases when the bi-metallic Pt-Ni or Pd-Ni cluster is established. In such situations, the laboratory operations become more and more reliable than 200 h.[14,39].

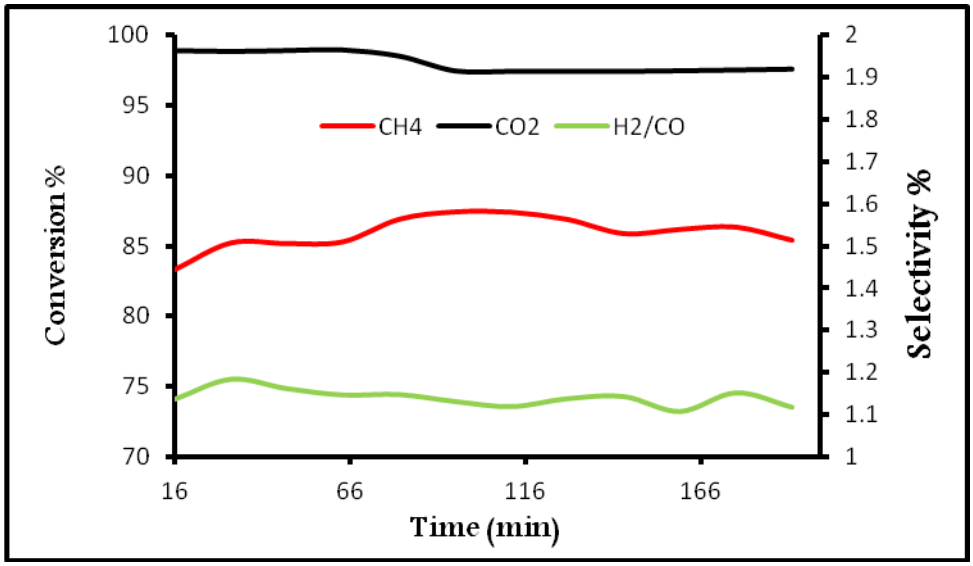

Fig. 7: Stability tests of Pt,Pd,Ni/$Ca_{0.85}$ $Zr^{4+}{}_{0.15}O$ catalysts at 900 °C for the 1:1 ratio of CH_4:CO_2, for 200 h. (GHSV = 15000 ml.gcat-1.h-1, atmospheric pressure)

4. Conclusion

In order to produce synthesis gas, dry reforming of methane was conducted on Ni Pd,Pt/Ca_{1-x} Zr_xO catalysts. The catalysts were fabricated using co-precipitation process with K_2CO_3 as precipitator. The XRD, H_2-TPR, BET, TEM and TGA catalysts have their physical and chemical properties. The most high activity was revealed by the Ni, Pd, Pt/$Ca_{0.85}Zr^{4+}{}_{0.15}O$ catalyst, resulting in supportive CO_2 and CH_4 conversion rates of 98.02 and 85.94 percent, and an adequate H_2/CO ratio of 1.14 at 900°C and 1:1 at CH_4:CO_2 temperature. The different results of catalysts disclosed that the catalytic properties of catalysts strongly rely on the type and concentration of the promoter. Catalyst stability Ni,Pd,Pt/ $Ca_{0.85}Zr^{4+}{}_{0.15}O$ was investigated for 200 hours.

Acknowledgements

Immense thanks should go to NanoMite Grant (Vot. No: 5526308) for the provision of the necessary funds for carrying out this study. I am fully indebted to Prof. Taufiq Yap Yun-Hin for unexampled assistance, feedback and support he made available during the time of this research.

References

[1] K. Sutthiumporn, T. Maneerung, S. Kawi, CO_2 dry-reforming of methane over $Zr_{0.8}Sr_{0.2}Ni_{0.8}M_{0.2}O_3$ perovskite (M= Bi, Co, Cr, Cu, Fe): roles of lattice oxygen on C-H activation and carbon suppression, Int. J. Hydro. E. 37(2012) 11195-11207.

[2] M.R. Rahimpour, Z.A. Aboosadi, A.H. Jahanmiri, Optimization of tri-reformer reactor to produce synthesis gas for methanol production using differential evolution (DE) method, Appl. Energy. 88 (2011) 2691-2701.

[3] M.A. Nabilah, N. Dai-Viet, M.T. Azizan, Z.A. Sumaia, Carbon dioxide dry reforming of glycerol for hydrogen production using Ni/ZrO_2 and Ni/CaO as catalysts, BCREC. 11 (2016) 200-209.

[4] M. Sarkari, F. Fazlollahi, H. Ajamein, H. Atashi, W.C Hecker,. L.L. Baxter, Catalytic performance of an iron-based catalyst in fischer–tropsch synthesis, Fuel Pro. Tech. 127 (2014) 163-170.

[5] B.V. Ayodele, M.R. Khan, C.K. Cheng, Production of CO-rich hydrogen gas from methane dry reforming over Co/CeO_2 catalyst, BCREC. 11(2016) 210-219.

[6] P. Gangadharan, K.C. Kanchi, H.H. Lou, Evaluation of the economic and environmental impact of combining dry reforming with steam reforming of methane, Chem. Eng. Res. 90 (2012) 1956-1968.

[7] J. Kehres, J.G. Jakobsen, J.W. Andreasen, J.B. Wagner, H. Liu, Molenbroek, A., Vegge, T. Dynamical properties of a Ru/$MgA_{l2}O_4$ catalyst during reduction and dry methane reforming, J. Ph. Chem. 116 (2012) 21407-21415.

[8] M. Garcia-Dieguez, I.S. Pieta, M.C. Herrera, M.A. Larrubia, L.J. Alemany, Rh-Ni nanocatalysts for the CO_2 and CO_2+H_2O reforming of methane, Catal. Today. 172 (2011) 136-142.

[9] F. Menegazzo, M. Signoretto, P. Canton, N. Pernicone, Optimization of bimetallic dry reforming catalysts by temperature programmed reaction, Appl. Catal. A. 439 (2012) 80-87.

[10] F.A. Al-Doghachi, U. Rashid, Y.H. Taufiq-Yap, Investigation of Ce (III) promoter effects on the tri-metallic Pt,Pd,Ni/MgO catalyst in dry-reforming of methane, RSC Adv. 6 (2016) 10372-10384.

[11] M. Yu, K. Zhu, Z. Liu, H. Xiao, X. Zhou, Carbon dioxide reforming of methane over promoted $Ni_xCa_{1-x}O$ (111) platelet catalyst derived from solvothermal synthesis, Appl. Catal. B, Environ. 148 (2014) 177-190.

[12] F.A. Al-Doghachi, U. Rashid, Z. Zainal, M.I Saiman,. Y.H. Taufiq-Yap, Influence of Ce_2O_3 and CeO_2 promoters on Pd/MgO catalysts in the dry-reforming of methane, RSC Adv. 5 (2015) 81739-81752.

[13] F.A. Al-Doghachi, A. Islam, Z. Zainal, M. I. Saiman, Z. Embong, Y.H. Taufiq-Yap, Hydrogen production from dry-reforming of biogas over Pt/Mg1-xNixO catalysts, E. Procardia. 79 (2015) 18-25.

[14] F. Liu, Y. Xiao, X. Sun, G. Qin, X. Song, Y. Liu, Synergistic catalysis over hollow CeO_2-CaO-ZrO_2 nanostructure for polycarbonate methanolysis with methanol, Chem. Eng. J. 369 (2019) 205-214.

[15] E.G. Mahoney, J. Pusel, W.S. Stagg, S. Faraji, The effects of Pt addition to supported Ni catalysts on dry (CO_2) reforming of methane to syngas, J. CO_2 Utilization. 6 (2014) 40-44.

[16] Z. Bao, Y. Lu, J. Han, Y. Li, F. Yu, Highly active and stable Ni-based bimodal pore catalyst for dry reforming of methane, Appl. Catal. A, Gen. 491 (2015) 116-126.

[17] B.S. Roberto, R.C. Juniora, N.R.S. Rabelo, F.B.N. Gomes, Steam reforming of acetic acid over Ni-based catalysts derived from $La_{1-x}Ca_xNiO_3$ perovskite type oxides, Fuel . 82 (2019) 20081-312

[18] S. Tada, T. Shimizu, H. Kameyama, T. Haneda, Ni/CeO_2 catalysts with high CO_2 methanation activity and high CH_4 selectivity at low temperatures, Int. J. Hydro. E. 37 (2012) 5527-5531.

[19] D.V. Gonzalez, F.M. Ternero, R. Peren, A. Caballero, J.P. Holgado, Study of nanostructured Ni/CeO_2 catalysts prepared by combustion synthesis in dry reforming of methane, Appl. Catal. A: General. 384 (2010) 1-9.

[20] K.Y. Koo, H.S. Roh, Y.T. Seo, D.J. Seo, W.L. Yoon, S.B. Park, A highly effective and stable nano-sized Ni/MgO-Al_2O_3 catalyst for gas to liquids (GTL) process, Int. J. Hydro. E.33 (2008) 20-36.

[21] F.A. Al-Doghachi, Effects of platinum and palladium metals on Ni/$Mg_{1-x}Zr_xO$ catalysts in the CO_2 reforming of methane, BCREC. 13 (2018) 295-310.

[22] A. J. Faris Y. H. Taufiq-Yap, CO_2 reforming of methane over Ni/MgO catalysts promoted with Zr and La oxides, Chem. sel. 3 (2018) 816-827.

[23] A. Djadja, S. Libs, A. Kiennemann, A. Barama, Characterization and activity in dry reforming of methane on Ni,Mg/Al and Ni/MgO catalysts, Catal. Today. 113 (2006) 194-200.

[24] W. Ahmed, A.E. Awadallah, E.A.A. Aboul, Ni/CeO_2-Al_2O_3 Catalysts for methane thermo-catalytic decomposition to CO_x-free H_2 production, Int. J. Hydro. E. 41 (2016) 18484-18493.

[25] E. P. Komarala, I. Komissarov, B. A. Rosen . Effect of Fe and Mn substitution in $LaNiO_3$ on ex solution, activity, and stability for methane dry reforming , catal. 10 (2019) 1001-0027 .

[26] A. Zecchina, G. Spoto, S. Coluccia, E. Guglielminotti, Spectroscopic study of the adsorption of carbon monoxide on solutions of nickel oxide and magnesium oxide. Part 2. Samples pretreated with hydrogen, J. Chem. Soc. 80 (1984) 1891-1901.

[27] Y.H. Hu, E. Ruckenstein, multiple transient tesponse methods to identify mechanisms of heterogeneous catalytic reactions, Acco. Chem. Res. 36 (2003) 791-797.

[28] S. Appari, V.M. Janardhanan, R. Bauri, S. Jayanti, O. Deutschmann, Detailed kinetic model for biogas steam reforming on Ni and catalyst deactivation due to sulfur poisoning, Appl. Catal. A: Gen. 471 (2014) 118-125.

[29] P. Djinović, G. Osojnik, B. Erjavec, A. Pintar, Influence of active metal loading and Oxygen mobility on coke-free dry reforming of Ni-Co bimetallic catalysts**,** Appl. Catal. B: Environ. 125 (2012) 259-270.

[30] P. Djinović, G. Osojnik, B. Erjavec, A. Pintar, Influence of active metal loading and Oxygen mobility on coke-free dry reforming of Ni-Co bimetallic catalysts, Appl. Catal. B: Environ.125 (2012) 259-270.

[31] A.S. Al-Fatesh, M.A. Naeem, A.H. Fakeeha, A.E. Abasaeed, CO_2 reforming of methane to produce syngas over γ-Al_2O_3- supported Ni-Sr catalysts, Bulletin of the Chem. Soc. of Japan. 2013. 86 742-748.

[32] A. Topalidis, D.E. Petrakis, A. Ladavos, L. Loakatzikou, P.J. Pomonis, A kinetic study of methane and carbon dioxide inter conversion over 0.5% Pt/$SrTiO_3$ catalysts, Catal. Today. 127 (2007) 238-245.

[33] K. Nakagawa, M. Kikuchi, M. Nishitani-Gamo, H. Oda, H. Gamo, Ogawa, K. Ando, T. CO_2 reforming of CH_4 over Co/oxidized diamond catalyst, E. & Fuels. 22 (2008) 3566-3570.

[34] T. Osaki, T. Mori, Role of potassium in carbon-free CO_2 reforming of methane on K-promoted Ni/Al_2O_3 catalysts, J. Catal. 204 (2001) 89-97.

[35] J. Kehres, J.G. Jakobsen, J.W. Andreasen, J.B. Wagner, H. Liu, A. Molenbroek, T. Vegge, Dynamical properties of a Ru/$MgAl_2O_4$ catalyst during reduction and dry methane reforming , J. Physic. Chem. 116 (2012) 21407-21415.

[36] F. Giordano, A. Trovarelli, C. Leitenburg, M. Giona, A model for the temperature-programmed reduction of low and high surface area ceria, Catal. 193 (2000) 273-282.

[37] B. Steinhauer, M. Kasireddy, J. Radnik, A. Martin, Development of Ni-Pd bimetallic catalysts for the utilization of carbon dioxide and methane by dry reforming**,** Appl. Catal. A: Gen. 366 (2009) 333-341.

[38] I. Istadi, D.D. Anggoro, N.A.S. Amin, D.H.W. Ling, Catalyst deactivation simulation through carbon deposition in carbon dioxide reforming over Ni/CaO-Al_2O_3 catalyst, BCREC. 6 (2011) 129-136.

[39] S. Miguel, I. Vilella, S. Maina, D.J. Alonso, M.R. Martinez, I.M. Gomez, Influence of Pt addition to Ni catalysts on the catalytic performance for long term dry reforming of methane. Appl. Catal. A: Gen. 435 (2012) 10-18.

المستخلص

تم تحضير العامل المساعد او (المحفز) ($Pt,Pd\ and\ Ni/Ca_{1-x}Zr_xO$) باستخدام طريقة الترسيب المشتركة (co-precipitation) بواسطة العامل المرسب (K_2CO_3) وتم تحميل الفلزات البلاتين , البلاديوم والنيكل على (CaO) و (ZrO_2) وبنسبة 1% لكل منهما لتحسين عمل العامل المساعد ($Pt,Pd\ and\ Ni/Ca_{1-x}Zr_xO$) حيث أن ($x = 0, 0.03, 0, 07\ and\ 0.15$) . بينما تم تشخيص صفات العامل المساعد المحضر من خلال (XRD), (H2-TPR) , (BET), (TEM), و (TGA) . وخلال الدراسة التي اجريت وجد ان المحفز ($Ni,Pd,Pt/Ca_{0.85}Zr^{4+}{}_{0.15}O$) هو اكثر فعالية مقارنة مع المحفزات الاخرى من حيث عمليات تحويل غاز الميثان وغاز ثنائي اوكسيد الكاربون , حيث كانت نسبة التحويل للميثان (85.94) و ثنائي اوكسيد الكاربون (98.02) بينما نسبة (H_2/CO) كانت (1.14) عند درجة حرارة 900 درجة مئوية ونسبة غاز الميثان الى غاز ثنائي اوكسيد الكاربون هي (1:1) . وعندما تم اضافة كمية من (ZrO_2) كداعم للمحفز ظهرت مجموعة من التأثيرات المختلفة منها : **اولا** اصبح الشكل المكعب لا وكسيد الكالسيوم اكثر استقرارا , **ثانيا** ازدياد الاستقرار الحراري للمحفز , **ثالثا** التقليل من عملية ترسيب الكاربون على سطح المحفز وكذلك قلت قابلية اختزال الايونات (Ni^{2+},) , (Pd^{2+}) و (Pt^{2+}) .